

SUZAKU X-RAY IMAGING OF THE EXTENDED LOBE IN THE GIANT RADIO GALAXY NGC 6251 ASSOCIATED WITH THE *FERMI*-LAT SOURCE 2FGL J1629.4+8236

Y. TAKEUCHI¹, J. KATAOKA¹, Ł. STAWARZ^{2,3}, Y. TAKAHASHI¹, K. MAEDA¹, T. NAKAMORI¹,
C. C. CHEUNG^{4,6}, A. CELOTTI⁵, Y. TANAKA², AND T. TAKAHASHI²

¹ Research Institute for Science and Engineering, Waseda University, 3-4-1 Okubo, Shinjuku, Tokyo 169-8555, Japan; uto_of_take@suou.waseda.jp

² Institute of Space and Astronautical Science (ISAS), Japan Aerospace Exploration Agency (JAXA),

3-1-1 Yoshinodai, Chuo-ku, Sagami-hara, Kanagawa 252-5510, Japan

³ Astronomical Observatory, Jagiellonian University, ul. Orla 171, Kraków 30-244, Poland

⁴ National Academy of Sciences, Washington, DC 20001, USA

⁵ Scuola Internazionale Superiore di Studi Avanzati (SISSA), 34014 Trieste, Italy

Received 2012 January 25; accepted 2012 February 1; published 2012 March 23

ABSTRACT

We report the results of a *Suzaku* X-ray imaging study of NGC 6251, a nearby giant radio galaxy with intermediate FR I/II radio properties. Our pointing direction was centered on the γ -ray emission peak recently discovered with the *Fermi* Large Area Telescope (LAT) around the position of the northwest (NW) radio lobe 15 arcmin offset from the nucleus. After subtracting two “off-source” pointings adjacent to the radio lobe and removing possible contaminants in the X-ray Imaging Spectrometer field of view, we found significant residual X-ray emission most likely diffuse in nature. The spectrum of the excess X-ray emission is well fitted by a power law with a photon index $\Gamma = 1.90 \pm 0.15$ and a 0.5–8 keV flux of 4×10^{-13} erg cm⁻² s⁻¹. We interpret this diffuse X-ray emission component as being due to inverse Compton upscattering of the cosmic microwave background photons by ultrarelativistic electrons within the lobe, with only a minor contribution from the beamed emission of the large-scale jet. Utilizing archival radio data for the source, we demonstrate by means of broadband spectral modeling that the γ -ray flux of the *Fermi*-LAT source 2FGL J1629.4+8236 may well be accounted for by the high-energy tail of the inverse Compton continuum of the lobe. Thus, this claimed association of γ -rays from the NW lobe of NGC 6251, together with the recent *Fermi*-LAT imaging of the extended lobes of Centaurus A, indicates that particles may be efficiently (re-)accelerated up to ultrarelativistic energies within extended radio lobes of nearby radio galaxies in general.

Key words: acceleration of particles – galaxies: individual (NGC 6251) – galaxies: jets – gamma rays: general – radiation mechanisms: non-thermal – X-rays: galaxies

Online-only material: color figures

1. INTRODUCTION

With the successful launch of the *Fermi* Gamma-ray Space Telescope, we now have an unprecedented opportunity to study in detail the γ -ray emission from different types of astrophysical sources. The 2FGL catalog (Abdo et al. 2012)⁷ contains 1873 sources detected in the 100 MeV to 100 GeV range by the Large Area Telescope (LAT) on board the *Fermi* satellite during the first 24 months of the science phase of the mission, which began on 2008 August 4. Among 1297 objects included in 2FGL, which are firmly identified or reliably associated with counterparts of known source classes, more than half are blazars, i.e., active galactic nuclei (AGNs) with radiative outputs dominated by a beamed jet emission. Non-blazar AGNs constitute only a small fraction ($\simeq 3\%$) of the identified 2FGL population, but nonetheless they have already emerged as a new, important, and at the same time relatively diverse, class of γ -ray emitters. The second catalog of AGNs detected by *Fermi*-LAT (2LAC; Ackermann et al. 2011) contains ten radio galaxies, four narrow-line Seyfert 1 galaxies, and several other nonblazar-type AGNs with prominent starburst components (see also Abdo et al. 2010c; Ackermann et al. 2012).

Particularly noteworthy in this context is the *Fermi*-LAT detection of the giant lobes in the nearby radio galaxy Centaurus A,

extending for about $\sim 5^\circ$ in the east–west direction and $\sim 9^\circ$ in the north–south direction (~ 300 kpc \times 600 kpc at the distance of 3.7 Mpc; Abdo et al. 2010b, 2010d). The *Fermi*-LAT results regarding the Centaurus A lobes have profound implications for the general understanding of the evolution of radio galaxies, their interactions with the surrounding environment, and the production of high-energy particles in the universe. In particular, prompted by these recent results from the *Fermi*-LAT and also from the Pierre Auger Observatory (Abraham et al. 2007; Moskalenko et al. 2009), several authors have debated on the high-energy particle acceleration and production of ultra high-energy cosmic rays within the giant lobes of Centaurus A and similar systems (Hardcastle et al. 2009; O’Sullivan et al. 2009; Pe’er & Loeb 2011).

Besides Centaurus A, three other radio galaxies detected so far with *Fermi*-LAT could be promising targets for investigating the extended γ -ray emission components associated with radio lobes. Prior to the launch of *Fermi*, Cheung (2007) and Georganopoulos et al. (2008) pointed out that the radio lobes of Fornax A might be detected at GeV energies and seen as extended structures by the LAT, but its associated 2FGL source is faint and currently appears to be a point source (Abdo et al. 2012). Similarly, the γ -ray emission associated with Centaurus B and reported recently in 2LAC may be dominated by the lobes, but, due to a relatively small angular size of the source (~ 0.2 in the north–south direction), careful analysis of the *Fermi*-LAT data is needed before drawing any robust conclusions (J. Katsuta et al. in preparation). The giant radio galaxy

⁶ National Research Council Research Associate; resident at Naval Research Laboratory, Washington, DC 20375, USA

⁷ See the online version at http://fermi.gsfc.nasa.gov/ssc/data/access/lat/2yr_catalog/.

Table 1
Suzaku XIS Observation Log

Target Name	R.A. (deg)	Decl. (deg)	Exposure (ks)	Obs. Start Time (UT)
NGC 6251_LOBE	246.5880	82.6370	34.2	2011 Apr 15 06:37:27
NGC 6251_LOBE_BGD1	247.8200	82.9170	18.8	2011 Apr 16 00:38:47
NGC 6251_LOBE_BGD2	245.4460	82.3530	12.1	2011 Apr 16 10:25:32

NGC 6251 already appeared in the first-year *Fermi*-LAT catalog (1FGL; Abdo et al. 2010a) and is another object worthy of attention due to the large angular extent of its radio structure ($\sim 1:2$), which, in principle, could be resolved with *Fermi*-LAT above 1 GeV photon energies. Based on the 1 yr of accumulated LAT data, the NGC 6251 nucleus was included within the 95% LAT error ellipse of 1FGL J1635.4+8228, and its reported γ -ray flux could be due to the unresolved nuclear jet of the radio galaxy (Migliori et al. 2011). Subsequently, however, the position of the 2FGL counterpart of NGC 6251, namely, 2FGL J1629.4+8236 (detected at the 12σ level), is now shifted northwest (NW), with respect to the 1FGL source position, toward the outer jet and radio lobe. We note that previously the NGC 6251 galaxy was proposed to be associated with the EGRET source 3EG J1621+8203 (Mukherjee et al. 2002).

NGC 6251 is a nearby AGN hosting a supermassive black hole with a mass, $M_{\text{BH}} \simeq (4\text{--}8) \times 10^8 M_{\odot}$ (Ferrarese & Ford 1999; Ho 2002). It is classified as an FR I radio galaxy (Laing et al. 1983) based on its jet morphology and monochromatic 178 MHz luminosity of $1.9 \times 10^{24} \text{ W Hz}^{-1} \text{ sr}^{-1}$ (Waggett et al. 1977), although the entire giant radio structure resembles more FR II or intermediate FR I/FR II systems (Schoenmakers et al. 2001). At a distance of $\sim 106 \text{ Mpc}$ ($z = 0.0247$, conversion scale $0.491 \text{ kpc arcsec}^{-1}$; Wegner et al. 2003), the linear extension of the lobes reads as $\simeq 2.1 \text{ Mpc}$, which is a larger physical size than that covered by the outer lobes of Centaurus A. The radio jet in NGC 6251, discussed in detail in Perley et al. (1984), is likely to be relativistic up to large distances from the core and observed at viewing angles $\theta_j \lesssim 40^\circ$, as suggested by the jet-to-counterjet brightness asymmetry on both pc and kpc scales. It can be divided into (1) the bright inner region within the first $\sim 120''$, (2) a faint central part extending from $\sim 120''$ up to $\sim 180''$, (3) the *outer region* flaring between $\sim 180''$ and $\sim 270''$, and (4) a curved and low surface brightness tail beyond $\sim 270''$. The outer jet region has been detected at X-ray frequencies by *ROSAT* (Birkinshaw & Worrall 1993; Mack et al. 1997a), *XMM-Newton*, and *Chandra* (Sambruna et al. 2004b; Evans et al. 2005). The origin of the detected jet X-ray emission is still an open question and different models have been discussed for such, including thermal emission (Mack et al. 1997a), beamed inverse Compton radiation (Sambruna et al. 2004b), and synchrotron process (Sambruna et al. 2004b; Evans et al. 2005). However, none of the previous X-ray observations pointed to either the NW or southeast lobe regions, separated by $\sim 0:3$ and $\sim 0:7$ from the NGC 6251 nucleus, respectively.

In this paper, we present the results of the newly conducted observations of NGC 6251 with the *Suzaku* X-ray satellite (Mitsuda et al. 2007), mainly in 2011 April. NGC 6251 was first observed by *Suzaku* in 2010 December (Evans et al. 2011), but these observations strictly targeted the nucleus of the radio galaxy. This time, the pointing direction was intentionally shifted 15 arcmin in the NW direction from the nucleus to study the γ -ray emission peak discovered with *Fermi*-LAT around the position of the NW radio lobe. In Section 2, we describe

the *Suzaku* observations and data reduction procedure. The results of the analysis are given in Section 3. The discussion and conclusions are presented in Sections 4 and 5, respectively.

2. SUZAKU OBSERVATIONS AND DATA REDUCTION

Suzaku is the ideal instrument for the intended study since it provides a low and stable non-X-ray background (NXB), particularly for diffuse sources (Mitsuda et al. 2007; Tawa et al. 2008). We have, therefore, observed the NW lobe in NGC 6251 for 34.2 ks (“on” pointing). In addition, two short observations (18.8 ks and 12.1 ks) were made in the vicinity of the radio lobe to estimate the background flux (“off” pointings). Hereafter, we denote these three observations as LOBE, BGD1, and BGD2, respectively, and the observation log is provided in Table 1. Both BGD1 and BGD2 observations were made just after the LOBE observation so that the long-term background fluctuation as well as any possible effects caused by the detector degradation could be minimized. In the case of BGD2, an additional short (11.1 ks) exposure was obtained in 2011 August, but these data were excluded from the analysis presented here to avoid possible artifacts related to the aforementioned problems. We have checked that the presented results do not change within statistical errors when the additional BGD2 data are included in the spectral analysis.

The observations were made with an X-ray Imaging Spectrometer (XIS; Koyama et al. 2007), which consists of four CCD cameras each placed in the focal plane of the X-ray Telescope (XRT; Serlemitsos et al. 2007), and with the Hard X-ray Detector (HXD; Kokubun et al. 2007; Takahashi et al. 2007). Each XIS covers an $18' \times 18'$ region on the sky, which is large enough to include the entire NW lobe within a single pointing image. On the other hand, since HXD is a nonimaging instrument with a large field of view $34' \times 34'$ (Takahashi et al. 2007) and we cannot discriminate between the hard X-ray emission from the nucleus (Evans et al. 2011) and possible emission from the extended NW radio lobe in the HXD data, we only use the imaging and spectral results obtained with XIS in this paper. One of the XIS sensors (XIS 1) has a back-illuminated (BI) CCD, while the other three (XISs 0, 2, and 3) utilize front-illuminated (FI) CCDs. Because of an anomaly in 2006 November, the operation of XIS2 has been terminated and we use only three CCDs. The XIS was operated in the normal full-frame clocking mode with the 3×3 or 5×5 editing mode.

In our *Suzaku* pointing, the relatively bright NGC 6251 nucleus was located well outside the field of view of the XIS. However, due to the relatively large point-spread function of the XRT on board *Suzaku* (half-power diameter of $\simeq 2:0$; Serlemitsos et al. 2007), the contamination of the NGC 6251 nucleus may still, in principle, affect the exposure of the NW radio lobe: the pointing center of our LOBE observation is separated by only $\sim 15'$ from the core. For this reason, we simulated the contamination effect using *xissim*. In the simulation, we assumed a point source at the position of

the nucleus characterized by a power-law continuum with the photon index, $\Gamma = 1.87$, and the normalization $K = 6.79 \times 10^{-4}$ photons $\text{keV}^{-1} \text{cm}^{-2} \text{s}^{-1}$ at 1 keV (corresponding to the 2–10 keV unabsorbed luminosity $2.8 \times 10^{42} \text{erg s}^{-1}$), as reported in Evans et al. (2011). We found that the expected net count rate (the XIS count rate for the “on” pointing subtracted by the background count rate estimated from the “off” pointings) for the region used in the spectral analysis (see Section 3.2 below) due to the core contamination is only $4.11 \times 10^{-4} \text{s}^{-1}$, while the total source net count rate is $6.40 \times 10^{-2} \text{s}^{-1}$. Hence, we conclude that the leakage effect is at a level of about 0.64%, so the stray light contamination from the NGC 6251 nucleus can be considered as negligible when analyzing the diffuse emission of the NW lobe.

We analyzed the screened XIS data and reduced them using the *Suzaku* software version 1.2. The screening was based on the following criteria: (1) only ASCA-grade 0, 2, 3, 4, 6 events were accumulated, while hot and flickering pixels were removed from the XIS image using the `sisclean` script (Day et al. 1998); (2) the time interval after the passage of South Atlantic Anomaly was greater than 60 s; (3) the object was at least 5° and 20° above the rim of the Earth (elevation; ELV) during night and day, respectively. In addition, we also selected the data with a cutoff rigidity larger than 6 GV. In the reduction and the analysis of the *Suzaku* XIS data, HEADAS software version 6.11 and a calibration databases (CALDB) released on 2009 September 25 were used. The XIS cleaned event data set was obtained in the combined 3×3 and 5×5 edit modes using `xselect`. We note that no spectral variability were observed in the XIS data and the imaging and spectral analyses are discussed in the next section.

3. X-RAY ANALYSIS

3.1. Image Analysis

We extracted the XIS images within the photon energy range of 0.4–10 keV from only the two FI CCDs (XIS 0, XIS 3) because the BI CCD (XIS1) has lower imaging quality. In the image analysis, we excluded calibration sources at the corner of the CCD chips. The images of the NXB were obtained from the night Earth data using `xisnxbgen` (Tawa et al. 2008). Since the exposure times for the original data were different from that of NXB, we calculated the appropriate exposure-corrected original and NXB maps using `xisexpmapgen` (Ishisaki et al. 2007). The corrected NXB images were next subtracted from the corrected original images. In addition, we simulated flat sky images using `xissim` (Ishisaki et al. 2007) and applied a vignetting correction. All the images obtained with XIS0 and XIS3 were combined and rebinned by a factor of four (CCD pixel size $24 \mu\text{m} \times 24 \mu\text{m}$, so that 1024×1024 pixels cover an $18' \times 18'$ region on the sky; Koyama et al. 2007). Throughout these processes, we also performed vignetting correction for all the XIS images for LOBE, BGD1, and BGD2. Finally, the images were smoothed with a Gaussian function with $\sigma = 0'.28$.

The resulting XIS images are shown in Figure 1, with 325 MHz radio contours of NGC 6251 (Mack et al. 1997b) and the 95% LAT error circle of 2FGL J1629.4+8236 overlaid. When comparing the LOBE, BGD1, and BGD2 images, one can clearly see an excess X-ray emission possibly associated with the NW radio lobe. The apparent enhancements at the edges of the XIS images are artifacts due to an insufficient exposure at the CCD edges caused by small fluctuation of attitude during the observation. Interestingly, at the sensitivity limit of these *Suzaku* observations, no excess X-ray emission was detected from the

bright radio hotspot located at the edge of the lobe. In the context of the study by Hardcastle et al. (2004), since NGC 6251 is a low power FR I/II source, the X-ray emission from the hotspot is expected to be dominated by the high energy tail of the synchrotron continuum rather than by the inverse Compton component. Specifically, the radio flux of the hotspot of 0.1 Jy at 1.5 GHz allows us to roughly estimate the expected X-ray flux by extrapolating the observed hotspot spectrum from lower frequencies as $\sim 2 \text{nJy}$. A point source at this flux level is easily detectable by *Chandra* or *XMM*, but our *Suzaku* nondetection is unsurprising due to the relatively poor angular resolution of the instrument combined with a relatively intense diffuse emission of the surrounding lobe.

3.2. Spectral Analysis

In the spectral analysis, we extracted photons from the arc-like source region in the LOBE pointing as shown in Figure 2. This “arc-like region” is part of a concentric ring centered at the radio core position of NGC 6251. There we excluded X-ray point sources detected by *ROSAT* (see Table 1 described in Mukherjee et al. 2002) as background contaminants, assuming the source region radii $2'$ (a typical half-power diameter of the XRT, as described above). We note that the origin of these X-ray features is still under debate; hence, it remains possible that they represent hotspot and enhancement related to the NW lobe itself. In our analysis, however, we removed all such bright X-ray spots, since the main objective of the paper is to detect and to characterize the *diffuse* X-ray emission component associated with the *diffuse* radio structure of the lobe. Similarly, we defined arc-like background regions for both BGD1 and BGD2 pointings using the same detector coordinates that were chosen for the LOBE source region. We extracted the spectra from LOBE, BGD1, and BGD2 source regions with `xselect` for each CCD (XIS 0, XIS 1, XIS 3). Spectral analysis and model fitting were performed with `xspec` version 12.7.0. To improve the statistics, the spectra of XIS0 and XIS3 were summed together using `mathpha`. Moreover, the spectra of BGD1 and BGD2 were summed for the same reason in the same way. Finally, we made redistribution matrix files (RMFs) and ancillary response files (ARFs) using `xisrmfgen` and `xissimarfgen` (Ishisaki et al. 2007), respectively.

Using these RMFs and ARFs, the corrected spectrum about energy response and the effective area of XIS were obtained. Figure 3 shows the resulting (background subtracted) spectrum of the LOBE pointing within the energy range 0.4–7.5 keV. The spectrum could be well fitted by a single power-law continuum with a photon index, $\Gamma = 1.90 \pm 0.15$, moderated only by the Galactic absorption. The Galactic hydrogen column density was fixed as $N_{\text{H}} = 5.54 \times 10^{20} \text{cm}^{-2}$ (Dickey & Lockman 1990). The value of $\chi^2/\text{dof} = 20.54/14$ indicates that this is a satisfactory model for the diffuse X-ray emission component of the NW lobe in NGC 6251. The details of the fitting results are summarized in Table 2. We note that the spectrum is also equally well reproduced by thin thermal plasma models (either bremsstrahlung and/or Raymond-Smith) moderated by Galactic absorption with a temperature of $kT \gtrsim 3.7 \text{keV}$. This is rather high compared with the thermal plasma of nearby elliptical galaxies (e.g., Matsushita et al. 2000). Moreover, the implied thermal pressure, $p_{\text{th}} \sim 2 \times 10^{-10} \text{dyn cm}^{-2}$, is more than four orders of magnitude larger than the minimum-energy nonthermal pressure of the lobes (see Section 4.2). We regard these parameters as unrealistic; hence, we conclude that the

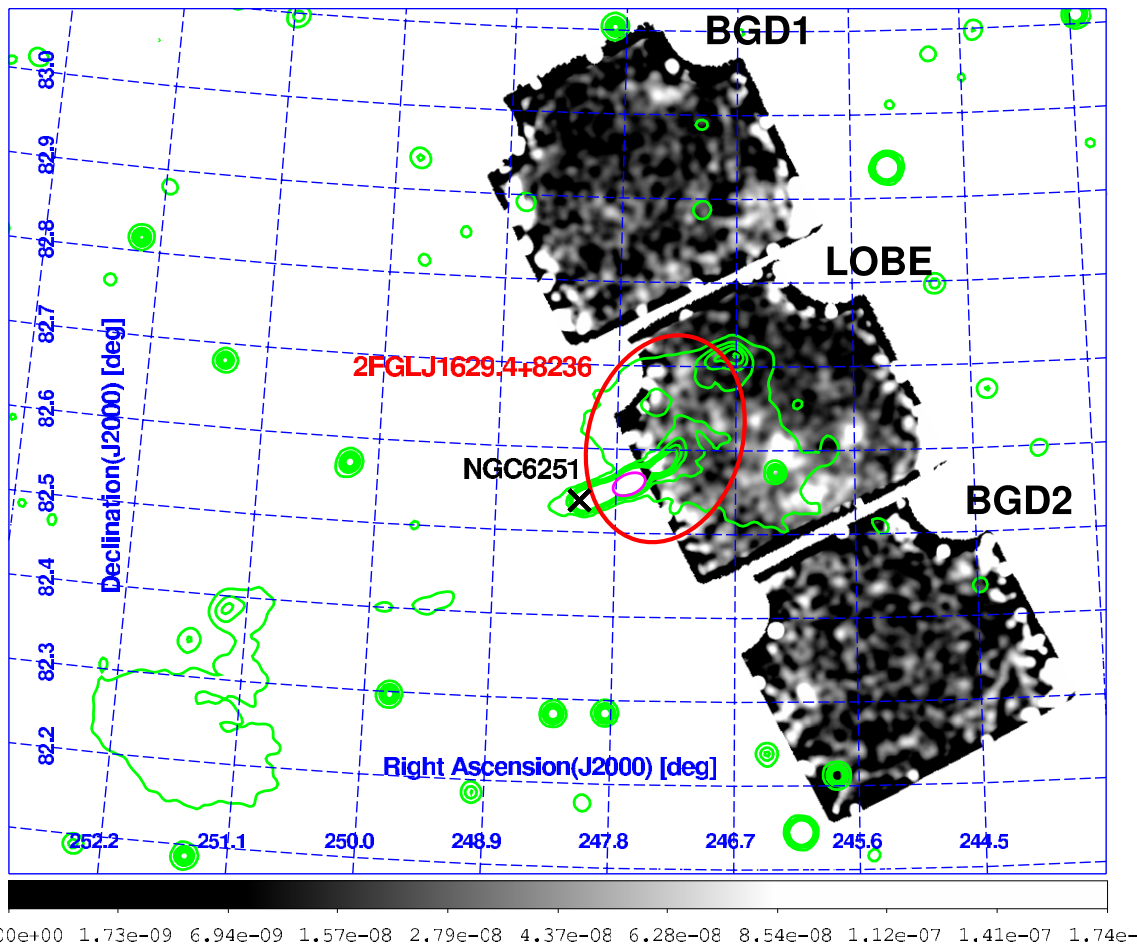


Figure 1. *Suzaku* X-ray image of the NW lobe in NGC 6251 (vignetting and exposure corrections applied). Data from XIS 0 and XIS 3 are summed in the 0.4–10 keV energy band. The image shows the relative excess of the smoothed photon counts (arbitrary units indicated in the bottom bar) and displayed with square root scaling. The green contours denote the large-scale radio structure of the source observed by *WSRT* at 55'' resolution (Mack et al. 1997b) and indicate levels of 8, 31, 54, 77, and 100 mJy beam⁻¹. The red ellipse denotes the 95% position error of 2FGL J1629.4+8236. The position of the radio core of NGC 6251 is marked by the black cross at the center, and the adjacent “outer jet region” is marked by the magenta ellipse.

(A color version of this figure is available in the online journal.)

Table 2
Fitting Parameters for the Power-law Model

Parameter	Value
N_{H} (cm ⁻²)	5.54×10^{20} (fixed)
Γ	1.90 ± 0.15
$K_{1\text{keV}}$ (keV ⁻¹ cm ⁻² s ⁻¹)	$(9.11 \pm 0.91) \times 10^{-5}$
χ^2/dof	20.54/14
$P(\chi^2)$	1.14×10^{-1}
$F_{0.4-7.5\text{keV}}$ (erg cm ⁻² s ⁻¹)	4.07×10^{-13}
$L_{0.4-7.5\text{keV}}$ (erg s ⁻¹)	5.4×10^{41}

diffuse X-ray emission component detected at the position of the NW lobe is purely nonthermal in origin.

4. DISCUSSION

The analysis of *Suzaku* data for the NW lobe in NGC 6251 revealed the presence of X-ray emission, most likely of diffuse nature, well fitted by a power-law continuum with a photon index $\Gamma \lesssim 2$ moderated only by the Galactic absorption. The 0.4–7.5 keV luminosity of the lobe corresponding to the *Suzaku* source extraction region reads as 5.4×10^{41} erg s⁻¹. The detection of such a nonthermal X-ray emission component is interesting, but not exceptional, since several analogous

detections of the X-ray lobes in either FR I or FR II radio galaxies have been previously reported (see Kataoka & Stawarz 2005; Croston et al. 2005; Isobe et al. 2011 and references therein). The relevance of our *Suzaku* observations of the NW lobe in NGC 6251 is due to the aforementioned possible (or even likely) association of the lobe with the *Fermi*-LAT source 2FGL J1629.4+8236. Note that, in the case of the only radio galaxy for which the lobe emission was robustly associated with a γ -ray source so far, Centaurus A, no diffuse X-ray emission component related to the extended radio structure has been detected (see Hardcastle et al. 2009). In other words, our observations may potentially provide the very first case of detected X-ray emission from a large-scale lobe bright in γ -rays.

Yet, the above statement may be considered premature, because the 95% LAT error circle of 2FGL J1629.4+8236 includes not only the extended lobe but also the bright “outer jet” region (see Section 1 and Figure 1). This region, as mentioned previously, has been resolved in X-rays before with *ROSAT*, *Chandra*, and *XMM-Newton* (Mack et al. 1997a; Sambruna et al. 2004b; Evans et al. 2005). Regardless of the debated origin of the jet-related X-ray photons (synchrotron versus beamed inverse Compton), large-scale jets detected at keV photon energies are, in general, thought to be the sites of efficient acceleration of high-energy electrons and, as such, may

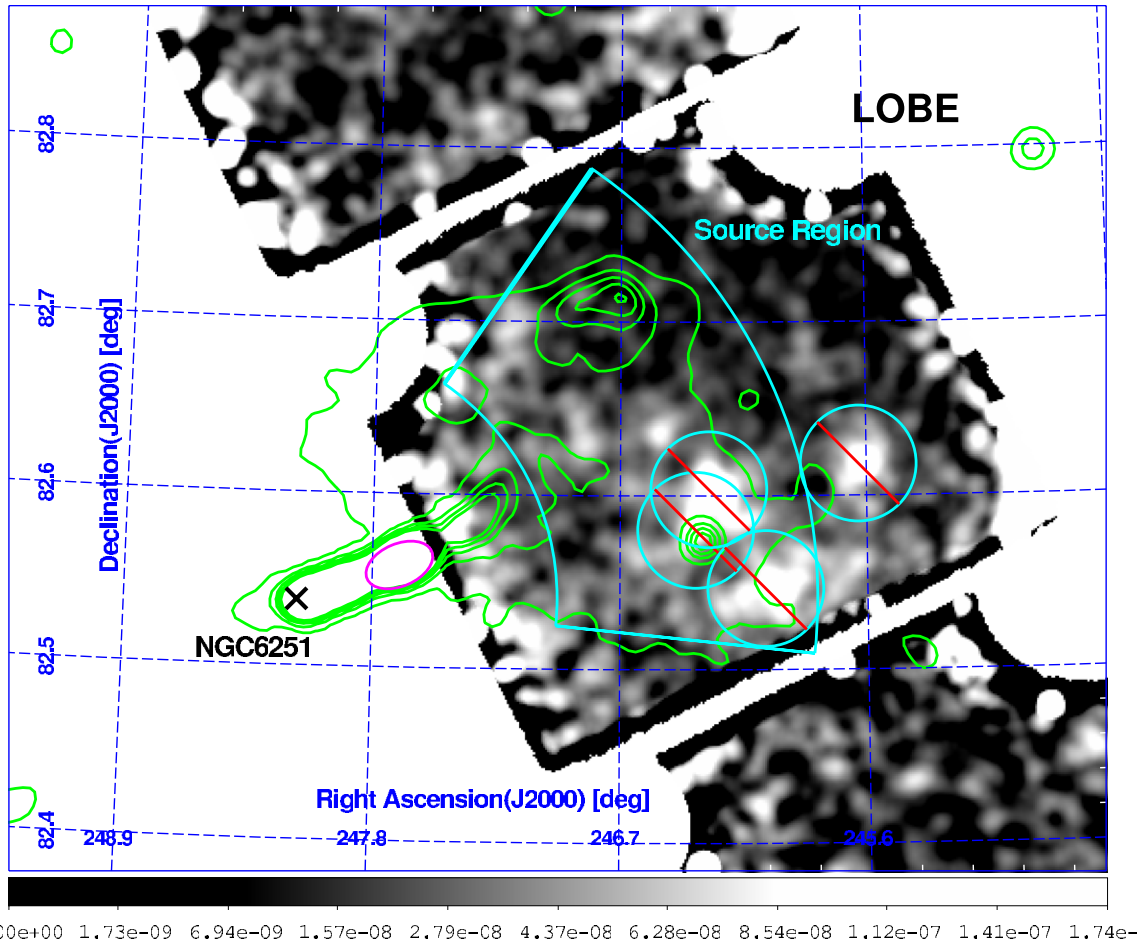


Figure 2. Same as Figure 1, but zooming into the NW lobe region. The *Suzaku* source extraction region is denoted by the cyan contours. The point X-ray sources removed from the analysis are marked by cyan circles with red stripes.

(A color version of this figure is available in the online journal.)

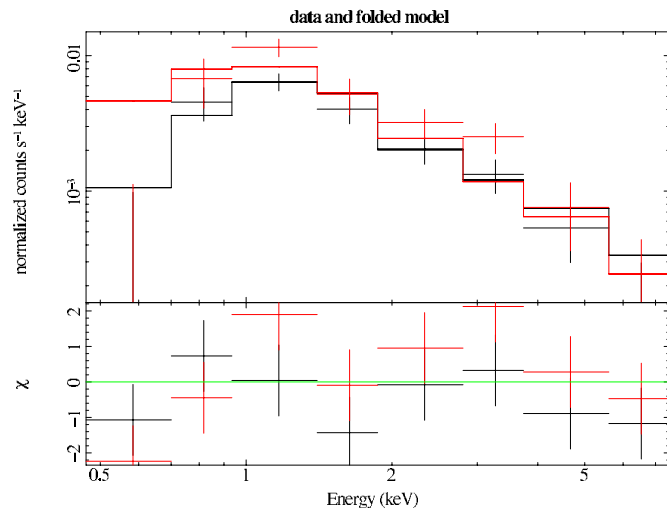


Figure 3. *Suzaku* XIS spectra of the diffuse emission component coinciding with the NW lobe of NGC 6251 in the photon energy range 0.4–7.5 keV, fitted by the model $wabs \times power-law$. The XIS0 + XIS3 and XIS1 spectra are shown in black and red, respectively.

(A color version of this figure is available in the online journal.)

be potential sources of γ -rays detectable by modern instruments like *Fermi*-LAT (see, e.g., Stawarz et al. 2004; Sambruna et al. 2004a). Below we discuss in more detail the possible association

of 2FGL J1629.4+8236 with the outer jet and the NW lobe of NGC 6251, and, through means of broadband spectral modeling, we demonstrate that the γ -ray flux can best be accounted for by the high-energy tail of the inverse Compton continuum of the lobe.

4.1. Outer Jet

For the spectral modeling of the outer jet region, we take the 1.4 GHz flux density, $S_{1.4\text{GHz}} = 0.5 \pm 0.05$ Jy, measured by Sambruna et al. (2004b) from a Very Large Array (VLA) map, and we assume the radio spectral index $\alpha_r = 0.64 \pm 0.05$ within the 1–5 GHz range (Perley et al. 1984). We also approximate the X-ray spectrum of this region as a power law with the photon index $\Gamma = 1.68 \pm 0.13$ within the 0.4–7 keV range and the monochromatic flux $S_{1\text{keV}} = 4.7 \pm 0.4$ nJy, as given in Evans et al. (2005).⁸ We approximate the jet as a cylinder with a radius $R_j = 5$ kpc and a *projected* length $\ell_j = 40$ kpc so that the emitting volume is $V_j = \pi R_j^2 \ell_j / \sin \theta_j$.

We model the broadband emission of the outer jet region in the framework of the beamed inverse Compton scenario (Tavecchio et al. 2000; Celotti et al. 2001). The radio emission is due to the synchrotron radiation of nonthermal electrons

⁸ We note that slightly different X-ray spectral parameters for the outer jet region are claimed by Sambruna et al. (2004b), namely, $S_{1\text{keV}} = 2.3 \pm 0.7$ nJy and $\Gamma = 1.15 \pm 0.38$ within the 0.5–9 keV range. Our reanalysis of archival *XMM-Newton* data is, however, more consistent with that of Evans et al. (2005).

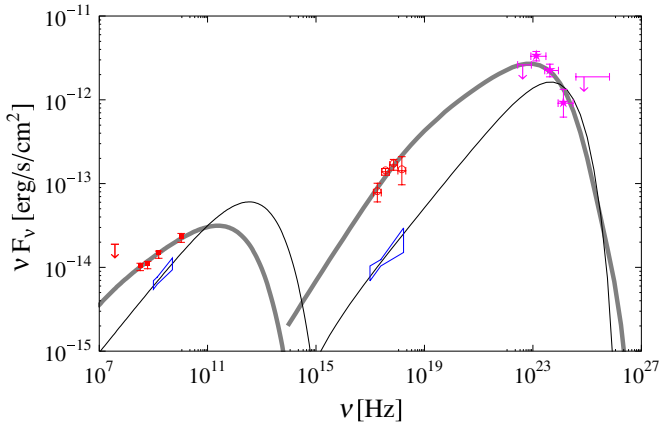


Figure 4. Broadband spectral energy distributions of the outer jet and the NW lobe in NGC 6251, including the *Fermi*-LAT source 2FGL J1629.4+8326. The radio and X-ray data for the outer jet (blue bow-ties) are from Sambruna et al. (2004b); based on the maps presented in Perley et al. (1984), and Evans et al. (2005), respectively (see Section 4.1). The radio fluxes of the NW lobe (red squares and red arrow) are described in Section 4.2. The X-ray fluxes for the lobe, as found in this paper, are given in the 0.5–1.0 keV, 1.0–2.0 keV, 2.0–4.0 keV, and 4.0–8.0 keV bins (open red circles). Finally, the LAT fluxes of 2FGL J1629.4+8326 are taken from the 2FGL catalog (Abdo et al. 2012). The thin solid line represents the beamed IC/CMB model for the outer jet (see Section 4.1), assuming an association with 2FGL J1629.4+8326. The thick gray line represents the IC/(CMB+EBL) model for the NW lobe (see Section 4.2), again assuming an association with 2FGL J1629.4+8326.

(A color version of this figure is available in the online journal.)

distributed isotropically within a relativistic outflow, and the X-ray-to- γ -ray continuum is due to Comptonization of the cosmic microwave background (CMB) photons by the same electron population (“beamed EC/CMB” model below). Anisotropy of the CMB radiation in the jet rest frame, as well as Klein–Nishina effects, is properly taken into account (Stawarz et al. 2005). For simplicity, we assume homogeneous distributions of the radiating electrons and of the magnetic field within the entire outer jet region, which should be considered as a rough approximation only considering the observed asymmetric radio intensity and polarization transverse profiles of the outer jet (Perley et al. 1984).

As shown in Figure 4 (thin solid line), the γ -ray flux of 2FGL J1629.4+8326 is not well accounted for by the beamed EC/CMB model for the jet with the following “best-fit” parameters: the ratio between comoving electron and magnetic field energy densities $\eta_{\text{eq}} \equiv U'_e/U'_B = 1.75$, magnetic field intensity $B = 2.3 \mu\text{G}$, jet bulk Lorentz factor $\Gamma_j = 3$, jet viewing angle $\theta_j = 17^\circ$, and the electron energy distribution of a power-law form $n'_e(\gamma) \propto \gamma^{-s} \times \exp[-\gamma/\gamma_{\text{max}}]$ with $s = 2.2$, $\gamma_{\text{min}} = 10$, and $\gamma_{\text{max}} = 5 \times 10^5$. With the above model parameters the observed ratio of the inverse Compton and synchrotron peak luminosities reads as $L_{\text{ic}}/L_{\text{syn}} \simeq (\delta/\Gamma_j)^2 \times (U'_{\text{cmb}}/U'_B) \simeq 25$. Note, however, that the relatively small jet viewing angle implied by the model, $\theta_j = 17^\circ$, may be considered unlikely when considering the large *projected* size of the whole radio structure of NGC 6251 (see the related discussion in Evans et al. 2005). On the other hand, the implied jet kinetic luminosities stored in electrons, magnetic field, and cold protons (assuming equal comoving number densities of protons and electrons), namely, $L_e \simeq 0.7 \times 10^{44} \text{ erg s}^{-1}$, $L_B \simeq 0.4 \times 10^{44} \text{ erg s}^{-1}$, and $L_p \simeq 1.9 \times 10^{45} \text{ erg s}^{-1}$, giving the total jet power $L_j \simeq 2 \times 10^{45} \text{ erg s}^{-1}$, could be considered as reasonable values (Willott et al. 1999). This may imply that, if the beamed

EC/CMB model for the large-scale jet in NGC 6251 with the parameters as given above is realistic at all, the outer parts of the outflow may provide some contribution to the observed γ -ray flux of 2FGL J1629.4+8326, at least at the highest photon energies within the LAT range.

4.2. NW Lobe

Next, we consider the case of the NW lobe of NGC 6251 likely associated with the *Fermi*-LAT source 2FGL J1629.4+8326. For the purpose of the spectral modeling we measured radio fluxes for the lobe from published *WSRT* maps at 327 and 610 MHz (Mack et al. 1997b). Additionally, we obtained a new VLA⁹ 1.56 GHz map at 45'' resolution with a total of 5 hr of integration from combining archival D-array observations obtained on 1985 December 1 and 5, and 1986 January 18 (programs AB346 and TEST). Our measurements, $S_{327\text{MHz}} = 3.10 \text{ Jy}$, $S_{610\text{MHz}} = 1.75 \text{ Jy}$, and $S_{1.56\text{GHz}} = 0.907 \text{ Jy}$, all assuming 10% errors, were measured using the same source extraction regions as in the *Suzaku* analysis (see Figure 2).¹⁰ The lobe also has a higher frequency radio flux measurement by Mack et al. (1997b), $S_{10.55\text{GHz}} = 213.5 \pm 26.4 \text{ mJy}$, and is detected and imaged down to 38 MHz (Rees 1990); due to the low resolution of the latter map, we summed the tabulated fluxes for the three components listed west of the central radio source to derive an upper limit to the lobe flux, $S_{38\text{MHz}} < 39.6 \text{ Jy}$. Note that the emerging radio spectral index $\alpha_{0.326-10.55\text{GHz}} \simeq 0.8$ is roughly consistent with the X-ray spectral index of the lobe measured by *Suzaku*. The lobe is approximated as a sphere with the radius $R_\ell = 185 \text{ kpc}$ so that the emission region volume is $V_\ell = (4/3)\pi R_\ell^3$.

For the lobe, we use a model similar to the outer jet region discussed above, but we also included extragalactic background light (EBL) photons within the infrared-to-optical range as a target photon field for the inverse Compton scattering (“EC/(CMB+EBL)” model). In the calculations, we use the EBL model of Mazin & Raue (2007) and account for Klein–Nishina effects. The choice of a particular EBL parameterization does not affect the model results because of the negligible contribution of the EC/EBL emission component to the γ -ray emission of the lobe within the LAT energy range. We neglect the contribution of the host galaxy to the target photon field because of the large distance of the analyzed NW lobe from the center ($15' \simeq 450 \text{ kpc}$). Finally, we assume homogeneous distributions of the radiating electrons and of the magnetic field within the lobe.

In the framework of the applied simplified model, the γ -ray flux of 2FGL J1629.4+8326 can be accounted for reasonably well (see the thick gray line in Figure 4) by the inverse Compton emission of the lobe for the following parameters: the equipartition ratio $\eta_{\text{eq}} \equiv U_e/U_B = 45$, magnetic field intensity $B = 0.37 \mu\text{G}$, and the electron energy distribution of a double-broken power-law form $n_e(\gamma) \propto \gamma^{-s_1}$ for $\gamma_{\text{min}} \leq \gamma \leq \gamma_{\text{br}}$ and $n_e(\gamma) \propto \gamma^{-s_2} \exp[-\gamma/\gamma_{\text{max}}]$ for $\gamma > \gamma_{\text{br}}$ with $s_1 = 2.0$, $s_2 = 2.5$, $\gamma_{\text{min}} = 1$, $\gamma_{\text{br}} = 3 \times 10^3$, and $\gamma_{\text{max}} = 10^6$. With the above model parameters, the lobe pressure stored in ultrarelativistic

⁹ Calibrated data sets obtained from the NRAO VLA Archive Survey. The National Radio Astronomy Observatory is a facility of the National Science Foundation operated under a cooperative agreement with Associated Universities, Inc.

¹⁰ The radio source extraction region includes a relatively bright radio hotspot mentioned already in Section 3.1. By means of careful analysis of the available radio maps, we have estimated the contribution of this hotspot to the total radio emission of the lobe as 10% at most, i.e., at the level of the assumed radio flux measurement uncertainty.

electrons and the magnetic field is $p_{e+B} \simeq 8.4 \times 10^{-14} \text{ dyn cm}^{-2}$. The total energy of the structure, being a sum of the work done when displacing a volume V_ℓ of surrounding gas at pressure p_{e+B} , namely, $p_{e+B} V_\ell$, and the energy of the material inside the cavity, $p_{e+B} V_\ell / (\hat{\gamma} - 1)$ (assuming ultrarelativistic equation of state with the adiabatic index $\hat{\gamma} = 4/3$), is then $E_{\text{tot}} \simeq 4 p_{e+B} V_\ell \sim 3 \times 10^{59} \text{ erg}$. The lobe's lifetime can be estimated as $t_\ell \sim E_{\text{tot}} / L_j \sim 10 \times (L_j / 10^{45} \text{ erg s}^{-1}) \text{ Myr}$. We note that any significant proton contribution to the lobe pressure would increase the evaluated values of E_{tot} and t_ℓ .

The EC/(CMB+EBL) model fits the data quite well, and the emerging lobe's parameters seem reasonable. The implied departure from the energy equipartition is rather large, $\eta_{\text{eq}} = 45$, but still within the range of 1–100, which was established for the lobes in radio galaxies with only X-ray measurements (e.g., Kataoka & Stawarz 2005; Croston et al. 2005; Isobe et al. 2011). Furthermore, the expected cooling timescale for the electrons emitting the observed $\gtrsim 1 \text{ GeV}$ photons, i.e., electrons with energies $\gamma \lesssim \gamma_{\text{max}} = 10^6$, is roughly $t_{\text{cool}} \simeq 2.1 \times (\gamma / 10^6)^{-1} \text{ Myr}$. Meanwhile, assuming a typical drift velocity of electrons in the lobe (or expansion velocity of the lobe) $v_{\text{lobe}} \lesssim 0.1c$, one can infer that these γ -ray emitting electrons can travel only $d \simeq 65 \times (v_{\text{lobe}} / 0.1c) \times (\gamma / 10^6)^{-1} \text{ kpc}$ before they cool radiatively. This scale is much smaller than the extension of the NW lobe in NGC 6251 ($\sim 0.5 \text{ Mpc}$). Interestingly, this finding resembles the case of the giant lobes in Centaurus A and similarly suggests an efficient in situ reacceleration of the radiating particles within the entire volume of the giant lobe (see the discussion in Abdo et al. 2010d). Moreover, in both the Centaurus A and NGC 6251 radio galaxies, the γ -ray detections imply that the lobes emit one to two orders of magnitude more energy in γ -rays than at radio/submm wavelengths.

Finally, we note that the nonthermal pressure of the NW lobe in NGC 6251, $\sim 10^{-13} \text{ dyn cm}^{-2}$, seems comparable with and a bit less than the thermal pressure of the surrounding gaseous medium, $p_{\text{th}} \sim (10^{-13} \text{ to } 10^{-12}) \text{ dyn cm}^{-2}$, at distances of $200''$ – $1000''$ from the core. The thermal pressure was estimated by Evans et al. (2005) based on the extrapolation of the X-ray halo profile associated with the group of galaxies, including NGC 6251, and detected by *Chandra* and *XMM-Newton* (see also Birkinshaw & Worrall 1993; Sambruna et al. 2004b). However, such an extrapolation may not provide a realistic estimate and should rather be considered as an upper limit for the ambient medium pressure. This, together with a likely contribution of (mildly) relativistic protons to the internal pressure of the lobe, may suggest that either the extended radio structures in NGC 6251 are in a pressure equilibrium with the environment or that these are overpressured cavities. Therefore, the expansion of the giant lobes in the system is still pressure driven on an Mpc scale (basically beyond the extension of the thermal halo of the surrounding group of galaxies).

5. CONCLUSIONS

We have presented a *Suzaku* X-ray observation of the NW lobe in a nearby radio galaxy, NGC 6251. Through this observation we found, for the first time, nonthermal diffuse X-ray emission associated with the NW lobe. Since the error circle of the γ -ray source 2FGL J1629.4+8236 contains *both* the NW lobe and the outer jet region, we discussed the possible origin of γ -ray emission using detailed modeling of the spectral energy distributions and assumed a synchrotron plus inverse Compton

emission on CMB background photons. We argued that, at least at energies below 10 GeV, the observed γ -ray emission is well explained by nonthermal emission from the NW lobe rather than from the outer jet region, with reasonable physical parameters (such as magnetic field, electron density, etc.) generally expected in radio lobes. Since the spatial extent of the NGC 6251 radio lobe is quite large ($\sim 0.5 \text{ Mpc}$), and the expected radiative cooling time is much shorter for γ -ray emitting electrons, efficient in situ acceleration of radiative particles is necessary within the entire volume of the giant lobe. We also briefly discussed the nonthermal pressure stored in ultrarelativistic electrons and the magnetic field (not considering a likely contribution of relativistic proton) of the NW lobe in NGC 6251, which is estimated as $\sim 10^{-13} \text{ dyn cm}^{-2}$ from the model. The lobe seems comparable with, or somewhat less than, the thermal pressure of the surrounding gaseous medium.

Ł.S. is grateful for the support from the Polish MNiSW through the grant N-N203-380336. C.C.C.'s work at NRL was supported by NASA DPR S-15633-Y.

REFERENCES

- Abdo, A. A., Ackermann, M., Ajello, M., et al. 2010a, *ApJS*, **188**, 405
 Abdo, A. A., Ackermann, M., Ajello, M., et al. 2010b, *ApJ*, **715**, 429
 Abdo, A. A., Ackermann, M., Ajello, M., et al. 2010c, *ApJ*, **720**, 912
 Abdo, A. A., Ackermann, M., Ajello, M., et al. 2010d, *Science*, **328**, 725
 Abdo, A. A., et al. 2012, *ApJS*, in press (arXiv:1108.1435)
 Abraham, J., Abreu, P., Aglietta, M., et al. (The Pierre Auger Collaboration) 2007, *Science*, **318**, 938
 Ackermann, M., Ajello, M., Allafort, A., et al. 2011, *ApJ*, **743**, 171
 Ackermann, M., Ajello, M., Allafort, A., et al. 2012, *ApJ*, in press (arXiv:1109.4678)
 Birkinshaw, M., & Worrall, D. M. 1993, *ApJ*, **412**, 568
 Celotti, A., Ghisellini, G., & Chiaberge, M. 2001, *MNRAS*, **321**, L1
 Cheung, C. C. 2007, in AIP Conf. Proc. 921, The First GLAST Symposium, ed. S. Ritz, P. Michelson, & C. A. Meegan (Melville, NY: AIP), **325**
 Croston, J. H., Hardcastle, M. J., Harris, D. E., et al. 2005, *ApJ*, **626**, 733
 Day, C., et al. 1998, The ASCA Data Reduction Guide, Technical Report, v.2.0 (Greenbelt, MD: NASA GSFC)
 Dickey, J. M., & Lockman, F. J. 1990, *ARA&A*, **28**, 215
 Evans, D. A., Hardcastle, M. J., Croston, J. H., Worrall, D. M., & Birkinshaw, M. 2005, *MNRAS*, **359**, 363
 Evans, D. A., Summers, A. C., Hardcastle, M. J., et al. 2011, *ApJ*, **741**, L4
 Ferrarese, L., & Ford, H. C. 1999, *ApJ*, **515**, 583
 Georganopoulos, M., Sambruna, R. M., Kazanas, D., et al. 2008, *ApJ*, **686**, L5
 Hardcastle, M. J., Cheung, C. C., Feain, I. J., & Stawarz, Ł. 2009, *MNRAS*, **393**, 1041
 Hardcastle, M. J., Harris, D. E., Worrall, D. M., et al. 2004, *ApJ*, **612**, 729
 Ho, L. C. 2002, *ApJ*, **564**, 120
 Ishisaki, Y., Maeda, Y., Fujimoto, R., et al. 2007, *PASJ*, **59**, 113
 Isobe, N., Seta, H., Gandhi, P., & Tashiro, M. S. 2011, *ApJ*, **727**, 82
 Kataoka, J., & Stawarz, Ł. 2005, *ApJ*, **622**, 797
 Kokubun, M., Makishima, K., Takahashi, T., et al. 2007, *PASJ*, **59**, 53
 Koyama, K., Tsunemi, H., Dotani, T., et al. 2007, *PASJ*, **59**, 23
 Laing, R. A., Riley, J. M., & Longair, M. S. 1983, *MNRAS*, **204**, 151
 Mack, K.-H., Kerp, J., & Klein, U. 1997a, *A&A*, **324**, 870
 Mack, K.-H., Klein, U., O'Dea, C. P., & Willis, A. G. 1997b, *A&AS*, **123**, 423
 Mazin, D., & Raue, M. 2007, *A&A*, **471**, 439
 Matsushita, K., Ohashi, T., & Makishima, K. 2000, *PASJ*, **52**, 685
 Migliori, G., Grandi, P., Torresi, E., et al. 2011, *A&A*, **533**, A72
 Mitsuda, K., Bautz, M., Inoue, H., et al. 2007, *PASJ*, **59**, 1
 Moskalenko, I. V., Stawarz, Ł., Porter, T. A., & Cheung, C. C. 2009, *ApJ*, **693**, 1261
 Mukherjee, R., Halpern, J., Mirabal, N., & Gotthelf, E. V. 2002, *ApJ*, **574**, 693
 O'Sullivan, S., Reville, B., & Taylor, A. M. 2009, *MNRAS*, **400**, 248
 Pe'er, A., & Loeb, A. 2011, arXiv:1111.3964
 Perley, R. A., Bridle, A. H., & Willis, A. G. 1984, *ApJS*, **54**, 291
 Rees, N. 1990, *MNRAS*, **244**, 233
 Sambruna, R. M., Gambill, J. K., Maraschi, L., et al. 2004a, *ApJ*, **608**, 698
 Sambruna, R. M., Gliozzi, M., Donato, D., et al. 2004b, *A&A*, **414**, 885

- Schoenmakers, A. P., de Bruyn, A. G., Röttgering, H. J. A., & van der Laan, H. 2001, *A&A*, **374**, 861
- Serlemitsos, P. J., Soong, Y., Chan, K.-W., et al. 2007, *PASJ*, **59**, 9
- Stawarz, Ł., Siemiginowska, A., Ostrowski, M., & Sikora, M. 2005, *ApJ*, **626**, 120
- Stawarz, Ł., Sikora, M., Ostrowski, M., & Begelman, M. C. 2004, *ApJ*, **608**, 95
- Takahashi, T., Abe, K., Endo, M., et al. 2007, *PASJ*, **59**, 35
- Tavecchio, F., Maraschi, L., Sambruna, R. M., & Urry, C. M. 2000, *ApJ*, **544**, L23
- Tawa, N., Hayashida, K., Nagai, M., et al. 2008, *PASJ*, **60**, 11
- Waggett, P. C., Warner, P. J., & Baldwin, J. E. 1977, *MNRAS*, **181**, 465
- Wegner, G., Bernardi, M., Willmer, C. N. A., et al. 2003, *AJ*, **126**, 2268
- Willott, C. J., Rawlings, S., Blundell, K. M., & Lacy, M. 1999, *MNRAS*, **309**, 1017